

Dynamic Interactive Buckling of Ring Stiffened Composite Shells

Andrea Schokker,* Akihito Kasagi,† and Srinivasan Sridharan‡
Washington University, St. Louis, Missouri 63130

The dynamic instability associated with the interactive buckling of ring stiffened composite shells under hydrostatic pressure is investigated. An optimally designed shell has its static local and overall buckling pressures close to one another. The shell response is then governed by the nonlinear interaction between the modes, which makes the shell very imperfection sensitive. A shell structure, such as a submarine vessel, can undergo suddenly applied overpressure or successive shocks. In the presence of imperfections, the dynamic instability will be triggered which would lead to a reduction of the load carrying capacity of the shell from that associated with quasistatic loading. Further, the large-amplitude vibrations that occur prior to reaching the dynamic limiting pressure can precipitate some form of material failure. The dynamic interactive buckling analysis developed in this study is a combination of the amplitude modulation technique and the asymptotic procedure. The nonlinear differential equations of motion for the structure so developed are solved by the Newmark method for time step integration along with Newton-Raphson iterations. Significant reductions in the load carrying capacity of the shells are observed as a combined result of the dynamic application of the load and the modal interaction. Damping was found to be of marginal influence in enhancing the dynamic limit load. Interlaminar stresses accompanying the dynamic response are monitored, and these reach significant values prior to the onset of dynamic instability.

Nomenclature

C_{ij}	= constitutive relation matrix	ρ	= mass density
d	= depth of stiffener below shell base	σ	= generic stress
E	= elastic modulus	τ	= shear stress
G	= shear modulus	ϕ	= shape function derived from Legendre polynomials
L	= shell length	ω	= frequency, rad/s
L_1, L_{11}, L_2	= linear, bilinear, and quadratic operators, respectively	$(\cdot)^{(0)}$	= prebuckling quantities
\mathcal{L}	= Langrange multiplier	$(\cdot)^{(1)}, (\cdot)^{(2)}$	= first- and second-order field quantities, respectively
m	= circumferential wave number for overall buckling	$(\cdot)_1, (\cdot)_2$	= overall quantities and local quantities, respectively
m_{ij}	= mass matrix	$(\cdot)_{12}$	= mixed second-order field quantities
N	= number of degrees of freedom		
N_1, N_2	= number of degrees of freedom in the determination of the buckling mode and the second-order field, respectively		
N_s	= number of stiffeners		
n	= circumferential wave number for local buckling		
q_0	= applied external pressure		
R_0, R, R_1	= inner, mean, and outer shell radii, respectively		
S_p	= spacing between stiffeners		
t	= shell thickness		
t_s	= stiffener thickness		
γ	= shear strain		
ϵ	= generic strain		
λ	= load parameter		
λ_{cr}	= critical value of λ		
$\lambda_{cr}^{(1)}, \lambda_{cr}^{(2)}$	= critical values corresponding to overall and local buckling, respectively		
λ_D	= dynamic limit load		
λ_2	= postbuckling coefficient		
ν	= Poisson's ratio		
Ξ_1	= $(\text{overall imperfection} \times 10^3)/R$		
Ξ_2	= $(\text{local imperfection} \times 10^2)/t$		
ξ	= scalar parameter which measures the growth of the buckling deformation		
$\tilde{\xi}$	= imperfection in the form of the buckling mode		

Received Aug. 18, 1994; revision received Feb. 24, 1995; accepted for publication Feb. 25, 1995. Copyright © 1995 by the American Institute of Aeronautics and Astronautics, Inc. All rights reserved.

*Graduate Student; currently at the Department of Aerospace Engineering and Engineering Mechanics, University of Texas, Austin, TX 78712.

†Postdoctoral Fellow; currently Structural Engineer, Engineering Applications Division, Kozo Keikaku Engineering Inc., Tokyo, Japan.

‡Professor.

Introduction

THE prospect of constructing submarine vessels of composite materials has led to a recent surge of interest in the compressive failure of composite cylinders. Although a certain amount of literature on instability of composite cylinders exists, the case of relatively thick composite shells has only recently received attention.¹ The problem of mode interaction of stiffened composite shells has been considered by Kasagi,² but the treatment is restricted to static pressures. Numerous studies on buckling and vibrations of composite cylindrical shells are available in the literature but are often limited to the case of unstiffened shells^{3,4} or consider only the free vibration problem.^{5,6} An early study on the phenomenon of dynamic stability of imperfection-sensitive structures was accomplished by Budiansky.⁷ This problem has since been treated extensively in literature, most notably by Simitses⁸ and his associates. More recently, dynamic instability of thick composite shells has been investigated by Palazotto et al.⁹

The behavior of ring stiffened composite shells is governed by two modes of buckling: the short wave local buckling mode occurring between stiffeners with a large number of waves in the circumferential direction (n) and the long wave overall mode consisting of a relatively small number of waves in the circumferential direction (m) in which the stiffeners are pulled in and out radially with the shell. An optimally designed shell structure is so proportioned that the critical stresses for these two cases is close and, thus, the principal cause of failure of an optimally designed shell is the adverse nonlinear interaction between the two modes. The present study deals with the dynamic instability associated with modal interaction in composite cylindrical shells. In particular, cylindrical shells with interior ring stiffeners are considered. A three-dimensional anisotropic elasticity formulation is employed in the analysis making it applicable for thick composite shells.

Problem Formulation

General Approach

As a first step, the principal modes of buckling that govern the static behavior are determined for the ring stiffened shells under hydrostatic pressure from a linear stability analysis, neglecting pre-buckling deformation. Next, the second-order fields associated with the individual modes as well as the mixed second-order field are determined using the perturbation technique. A three-dimensional finite element discretization is employed to extract these displacement fields. Thus, the displacements of the shell are expressible in terms of essentially two degrees of freedom, ξ_1 and ξ_2 , viz., the scalar parameters describing the growth of overall and local modes, respectively, in the total deformation. It has been shown,¹⁰⁻¹² however, that the amplitude of the local mode varies spatially as it comes under the influence of the overall mode. This is known as the amplitude modulation and has been accounted for in the present work. Thus, the deformation at any instant can be expressed in terms of ξ_1 and ξ_{ij} , where the latter are the arbitrary parameters that describe the spatial variation of the local buckling amplitude. Such a description of deformation in terms of parameters associated with static buckling in the investigation of dynamic instability implies the assumption that the excitation of the structure takes place in terms of the principal modes of buckling rather than the lowest modes of vibration. The nonlinear equations of motion of the structure are derived by formulating the potential energy and kinetic energy functions, respectively, and invoking the Lagrange equations of motion. Initial imperfections in the modes of buckling are readily incorporated in the potential energy expression by adding appropriate linear terms. For any given level of hydrostatic pressure, the solution of the equations is achieved in the time domain to give the dynamic response.

Shell Geometry and Material Properties

The shell coordinate system is shown in Fig. 1. The principal material directions of the lamina are given by the 1, 2, 3 coordinate system where the 1-2 axes are obtained by rotating both the longitudinal and circumferential tangents by an angle α . The 3 axis corresponds to the outward normal at any point. The coordinate system for the cylinder is defined by the longitudinal (x axis), radial (r axis), and circumferential (θ axis) directions. The displacements in the longitudinal, circumferential, and radial directions are given by u , v , and w , respectively. The stress-strain relationship for the material in the $x-r-\theta$ coordinate system is given by the following:

$$\left\{ \begin{array}{l} \sigma_1 \\ \sigma_2 \\ \sigma_3 \\ \sigma_4 \\ \sigma_5 \\ \sigma_6 \end{array} \right\} = \left[\begin{array}{cccccc} C_{11} & C_{12} & C_{13} & 0 & 0 & C_{16} \\ C_{12} & C_{22} & C_{23} & 0 & 0 & C_{26} \\ C_{13} & C_{23} & C_{33} & 0 & 0 & C_{36} \\ 0 & 0 & 0 & C_{44} & C_{45} & 0 \\ 0 & 0 & 0 & C_{45} & C_{55} & 0 \\ C_{16} & C_{26} & C_{36} & 0 & 0 & C_{66} \end{array} \right] \left\{ \begin{array}{l} \epsilon_1 \\ \epsilon_2 \\ \epsilon_3 \\ \epsilon_4 \\ \epsilon_5 \\ \epsilon_6 \end{array} \right\} \quad (1)$$

where the subscripts 1-6 are defined as follows for the shell: 1 $\rightarrow x$, 2 $\rightarrow \theta$, 3 $\rightarrow r$, 4 $\rightarrow r\theta$, 5 $\rightarrow rx$, and 6 $\rightarrow \theta x$; and for the stiffener: 1 $\rightarrow r$, 2 $\rightarrow \theta$, 3 $\rightarrow x$, 4 $\rightarrow \theta x$, 5 $\rightarrow rx$, and 6 $\rightarrow r\theta$.

For the stiffeners, we set $\sigma_x = 0$ and appropriately modify C_{ij} . The applied loads are hydrostatic and are made up of two parts: an axial force P and a radial pressure q_0 , as shown in Fig. 1a.

Details of the Finite Element Model

All of the finite element calculations are performed using the p -version technique, i.e., using the smallest possible number of elements and a set of hierarchic polynomials for the displacement functions to arrive at convergence. Thus, we adopt the discretization scheme shown in Fig. 1b consisting of three types of elements, viz., the bay, the stiffener, and the junction, and use the same scheme for the computation of prebuckling stress distribution, the buckling modes, and the second-order fields. The shape functions employed are derivable from Legendre polynomials¹³ and have been used by the authors in previous work.¹ Whereas these are employed in the longitudinal and thickness directions, "exact" trigonometric

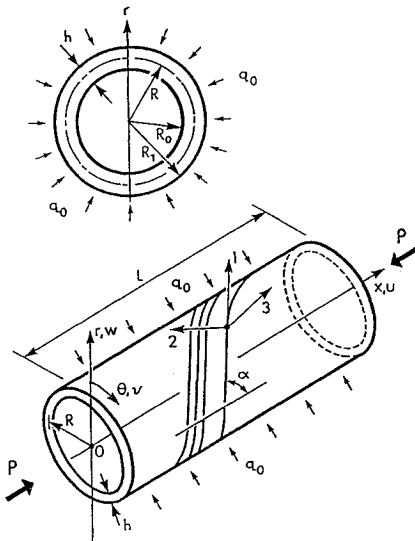


Fig. 1a Shell coordinate system, loading and fiber orientation.

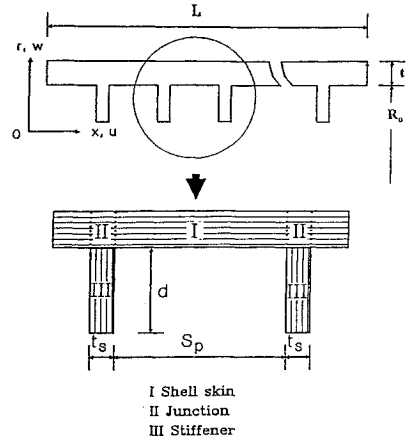


Fig. 1b Longitudinal section, stiffener geometry, and finite element discretization.

functions are employed in the circumferential direction. A three-dimensional formulation is used in terms of the three displacement components, and complete compatibility between the stiffener and shell is ensured.

Prebuckling

Prebuckling stresses are computed using the linear theory and assuming axisymmetric distribution in the sense of independence of θ . The corresponding displacements ($u^{(0)}$) are treated as infinitesimally small so that for any u , $L_{11}(u^{(0)}, u) = 0$, where L_{11} is a bilinear operator in the sense of Budiansky⁷ [also see Eq. (5)].

Total Potential Energy of the Buckled State of the Perfect Structure

Strain displacement relations are taken as follows. For the shell

$$\begin{aligned} \epsilon_r &= \frac{\partial w}{\partial r} \\ \gamma_{\theta x} &= \frac{\partial v}{\partial x} + \frac{1}{r} \frac{\partial u}{\partial \theta} + \frac{1}{r} \left[\left(\frac{\partial w}{\partial \theta} - v \right) \left(\frac{\partial w}{\partial x} \right) + w \left(\frac{\partial v}{\partial x} \right) \right] \\ \epsilon_{\theta} &= \frac{1}{r} \frac{\partial v}{\partial \theta} + \frac{w}{r} + \frac{1}{2r^2} \left[\left(\frac{\partial w}{\partial \theta} - v \right)^2 + \left(\frac{\partial v}{\partial \theta} + w \right)^2 \right] \\ \gamma_{rx} &= \frac{\partial u}{\partial r} + \frac{\partial w}{\partial x} \\ \epsilon_x &= \frac{\partial u}{\partial x} + \frac{1}{2} \left(\frac{\partial w}{\partial x} \right)^2 & \gamma_{r\theta} &= \frac{1}{r} \frac{\partial w}{\partial \theta} + \frac{\partial v}{\partial r} - \frac{v}{r} \end{aligned} \quad (2)$$

For the stiffener

$$\begin{aligned}\epsilon_r &= \frac{\partial w}{\partial x} + \frac{1}{2} \left[\left(\frac{\partial u}{\partial r} \right)^2 + \left(\frac{\partial w}{\partial r} \right)^2 \right] & \gamma_{\theta x} &= \frac{\partial v}{\partial x} + \frac{1}{r} \frac{\partial u}{\partial \theta} \\ \epsilon_\theta &= \frac{1}{r} \frac{\partial v}{\partial \theta} + \frac{w}{r} + \frac{1}{2r^2} \left[\left(\frac{\partial u}{\partial \theta} \right)^2 + \left(\frac{\partial w}{\partial \theta} \right)^2 \right] & (3) \\ \gamma_{rx} &= \frac{\partial u}{\partial r} + \frac{\partial w}{\partial x} \\ \epsilon_{r\theta} &= \frac{1}{r} \frac{\partial w}{\partial \theta} + \frac{\partial v}{\partial r} - \frac{v}{r} + \frac{1}{r} \left[\left(\frac{\partial u}{\partial r} \right) \left(\frac{\partial u}{\partial \theta} \right) + \left(\frac{\partial w}{\partial r} \right) \left(\frac{\partial w}{\partial \theta} \right) \right]\end{aligned}$$

These equations are valid for both the overall and local buckling problems. For local buckling the stiffeners undergo negligible translation in the radial direction and, thus, quadratic terms in w are of little significance. However, these terms are vital for describing overall buckling. The strain-displacement relations can be expressed in the general form

$$\{\epsilon\} = L_1(\mathbf{u}) + \frac{1}{2} L_2(\mathbf{u}) \quad (4)$$

where L_2 is a quadratic operator. A bilinear operator L_{11} needed later on is defined as follows:

$$L_2(\mathbf{u} + \mathbf{v}) = L_2(\mathbf{u}) + 2L_{11}(\mathbf{u}, \mathbf{v}) + L_2(\mathbf{v}) \quad (5)$$

Next, $\{\mathbf{u}\}$, $\{\epsilon\}$, and $\{\sigma\}$ can be viewed as being made up of two parts, one associated with the prebuckled state and one associated with buckling (asterisk quantities)

$$\begin{aligned}\{\mathbf{u}\} &= \{\mathbf{u}^{(0)}\} + \{\mathbf{u}^*\} \\ \{\epsilon\} &= \{\epsilon^{(0)}\} + \{\epsilon^*\} \\ \{\sigma\} &= \{\sigma^{(0)}\} + \{\sigma^*\}\end{aligned} \quad (6)$$

The total potential energy function governing the buckled state is then expressed from the stress-strain and strain-displacement relationships as

$$\begin{aligned}\Pi &= \frac{1}{2} \left[C_{ij} \{ L_{1ik}(u_k^*) \cdot L_{1ji}(u_i^*) + L_{1ik}(u_k^*) \cdot L_{2ji}(u_l^*) \right. \\ &\quad \left. + \frac{1}{4} L_{2ik}(u_k^*) \cdot L_{2ji}(u_l^*) \right] + \lambda \sigma_i^{(0)} \cdot L_{2ik}(u_k^*) \\ (i, j &= 1, 2, \dots, 6) \quad (k, l = 1, 2, 3) \quad (7)\end{aligned}$$

The equations of equilibrium are then found by rendering the potential energy function stationary.

Fluid Pressure Loading

In the present study, fluid pressure is realistically modeled as always directed normal to the surface during deformation ("live" pressure) in contrast to the radially directed "dead" pressure. This live fluid pressure loading case is still conservative, and a potential energy function can be written. The additional terms which arise to account for the potential energy due to live fluid pressure loading are as follows¹⁴:

$$\begin{aligned}V_p &= \frac{1}{2} q_0 \int \int \left[w \left(\frac{\partial u}{\partial x} \right) - \left(\frac{\partial w}{\partial x} \right) u + \frac{1}{R_1} \left\{ v^2 - v \left(\frac{\partial w}{\partial \theta} \right) \right. \right. \\ &\quad \left. \left. + \left(\frac{\partial v}{\partial \theta} \right) w + w^2 \right\} \right] R_1 dx d\theta \quad (8)\end{aligned}$$

where u , v , and w are the displacement components at the outer surface of the shell. These terms must be added to those in Eq. (9) to produce the total potential energy of the buckled structure. Note that the discrepancy between the radial and fluid pressure loading cases diminishes as the number of circumferential waves of buckling increases.

Asymptotic Procedure

The asymptotic approach developed by Koiter¹⁵ is used for the determination of the second-order fields associated with each of the modes of buckling. Displacement, strain, and stress are expressed in terms of an asymptotic expansion,

$$\begin{aligned}\{\mathbf{u}^*\} &= \{\mathbf{u}^{(1)}\} \xi + \{\mathbf{u}^{(2)}\} \xi^2 + \{\mathbf{u}^{(3)}\} \xi^3 + \dots \\ \{\epsilon^*\} &= \{\epsilon^{(1)}\} \xi + \{\epsilon^{(2)}\} \xi^2 + \{\epsilon^{(3)}\} \xi^3 + \dots \\ \{\sigma^*\} &= \{\sigma^{(1)}\} \xi + \{\sigma^{(2)}\} \xi^2 + \{\sigma^{(3)}\} \xi^3 + \dots\end{aligned} \quad (9)$$

where ξ is the scaling parameter of the buckling mode and measures its growth in the postbuckling deformation. Terms up to the second-order field are considered in the present study. By substitution of these equations into the equilibrium equation, viz., $\delta \Pi = 0$, and collecting terms associated with like powers of ξ , the following set of ordered perturbation equations is found:

$$\begin{aligned}\delta \Pi^{(1)} &= 0 \\ \delta \Pi^{(2)} &= 0\end{aligned} \quad (10)$$

where $\Pi^{(1)}$ and $\Pi^{(2)}$ are defined subsequently. The first-order set of the preceding equations [Eqs. (10)] is an eigenvalue problem; the solution of which gives the buckling load and mode, which are needed for handling the second-order set. An orthogonality condition between the sets is imposed; however, the choice of displacement functions in the present study results in the orthogonality condition being automatically satisfied. We choose the maximum amplitude at the center of the shell as the scaling parameter ξ and the buckling mode is normalized so as to make this parameter unity.

Buckling Problem

The potential energy for the first-order field is expressed as

$$\Pi^{(1)} = \frac{1}{2} \left[C_{ij} L_{1ik}(u_k^{(1)}) \cdot L_{1ji}(u_i^{(1)}) + \lambda \sigma_i^{(0)} \cdot L_{1ik}(u_k^{(1)}) \right] + V_p^{(1)} \quad (11)$$

where $V_p^{(1)}$ is quadratic in surface displacements. The exact displacement functions can be shown to take the form

$$\{u^{(1)}\} = \{u^{1S}(r, x)\} \sin(p\theta) + \{u^{1C}(r, x)\} \cos(p\theta) \quad (12)$$

where p is the wave number ($= m$ and n for the overall and local modes, respectively) and the functions $\{u^{1S}\}$ and $\{u^{1C}\}$ can be expressed in terms of the degrees of freedom u_{ij} , v_{ij} , and w_{ij} and the shape functions $\phi_i(r)$, $\phi_j(x)$. In terms of the generic degrees of freedom q_i , $\Pi^{(1)}$ takes the form

$$\Pi^{(1)} = \frac{1}{2} (\alpha_{ij}^{(1)} - \lambda b_{ij}^{(1)}) q_i^{(1)} q_j^{(1)} \quad (i, j = 1, 2, \dots, N_i) \quad (13)$$

where N_1 is the total number of degrees of freedom of the first-order problem. The equations of equilibrium then are found by rendering the potential energy function stationary.

This process is repeated for the second order field problem. First, a potential energy expression for the problem is invoked,

$$\begin{aligned}\Pi^{(2)} &= \frac{1}{2} \left[C_{ij} L_{1ik}(u_k^{(2)}) \cdot L_{1ji}(u_i^{(2)}) + \lambda \sigma_i^{(0)} \cdot L_{2ik}(u_k^{(2)}) \right. \\ &\quad \left. + C_{ij} \{ L_{2ik}(u_k^{(1)}) \cdot L_{1ji}(u_i^{(2)}) \right. \\ &\quad \left. + 2 L_{1ik}(u_k^{(1)}) \cdot L_{11j}(u_l^{(1)}, u_l^{(2)}) \} \right] + V_p^{(2)} \quad (14)\end{aligned}$$

where once again the V_p term is quadratic in second-order displacements. The displacement functions are taken in their exact form¹

$$\begin{aligned}\{u^{(2)}\} &= \{u^{20}(r, x)\} + \{u^{2S}(r, x)\} \sin(2p\theta) \\ &\quad + \{u^{2C}(r, x)\} \cos(2p\theta)\end{aligned} \quad (15)$$

The potential energy function in terms of the generic degrees of freedom takes the form

$$\begin{aligned}\Pi^{(2)} &= \frac{1}{2} (a_{ij}^{(2)} - \lambda b_{ij}^{(2)}) q_i^{(2)} q_j^{(2)} + c_{irs} q_i^{(2)} q_r^{(1)} q_s^{(1)} \\ (i, j &= 1, 2, \dots, N_2) \quad (r, s = 1, 2, \dots, N_1) \quad (16)\end{aligned}$$

The equations of equilibrium follow:

$$(a_{ij}^{(2)} - \lambda b_{ij}^{(2)})q_j^{(2)} = -c_{irs}q_i^{(1)}q_s^{(1)} \quad (17)$$

This set of equations is solved for $q_j^{(2)}$ by setting $\lambda = \lambda_{cr}$.

Static Postbuckling Response in the Individual Modes

Using the foregoing expressions [Eqs. (7), (9), (12), and (15)] it is possible to construct a potential energy function in terms of a single variable ξ in the form

$$\Pi = \frac{1}{2}(a - \lambda b)\xi^2 + c\xi^3 + d\xi^4 \quad (18)$$

where a , b , c , and d are constants calculable from the buckling modes and second-order field.^{1,15} Since the shell buckles into an integer number of full waves, $c = 0$. Thus, the bifurcation is symmetric. The equilibrium equation that gives the postbuckling response is given in the following form:

$$\lambda/\lambda_{cr} = 1 + \lambda_2(\xi/t)^2$$

where

$$\lambda_{cr} = a/b \quad \lambda_1 = 4t^2d/a \quad (19)$$

A positive value of λ_2 indicates a stable buckling process, whereas a negative value indicates an unstable process which leads to imperfection sensitivity. Results of such an analysis have been discussed by Kasagi and Sridharan¹ and Kasagi² and will not be discussed here any further.

Interactive Buckling

Amplitude Modulation

As a result of the interaction of the two fundamental modes of buckling, additional patterns of deformation are generated. These are given to first-order accuracy by the mixed second-order field ($\xi_1\xi_2$ field). It can be shown that this field consists principally of displacement fields in the form of local modes of buckling with wave numbers $n - m$ and $n + m$, where n and m are the local and overall buckling wave numbers, respectively. When $n \gg m$, the evaluation of this field using the standard perturbation procedure is riddled with singularities. This scenario is circumvented by the technique of amplitude modulation.

In the present treatment, an amplitude modulated local mode is employed, i.e., the scalar parameter representing the magnitude of the local buckling displacements is allowed to vary in the circumferential and axial directions according to a slowly varying function.¹⁰ Physically, the amplitude modulating function accentuates the displacement amplitudes on the compression side of overall mode while at the same time decreasing the amplitude on the tension side. The amplitude modulated local mode is equivalent to a linear combination of neighboring local modes with wave numbers, $\dots, n - m, n, n + m, \dots$, and it has two effects: it eliminates the singularity problem alluded to earlier and seriously diminishes the role of the mixed second-order field in the analysis.¹³

The mixed second-order field is evaluated, rendering the potential energy function stationary and imposing orthogonality to the local buckling modes with $n - m$ and $n + m$ waves, respectively, which are included by proxy in the amplitude modulated (first-order) local field. Symbolically this function is written as

$$\begin{aligned} \Pi_{12}^{(2)} = & \frac{1}{2}C_{ij} \left[L_{1ik} \left(u_{12k}^{(2)} \right) + 2 \left\{ L_{1ik} \left(u_{12k}^{(2)} \right) \cdot L_{11j} \left(u_{1i}^{(1)}, u_{2i}^{(1)} \right) \right. \right. \\ & + L_{1ik} \left(u_{1k}^{(1)} \right) \cdot L_{11j} \left(u_{2i}^{(1)}, u_{12i}^{(2)} \right) + L_{1ik} \left(u_{2k}^{(1)} \right) \cdot L_{11j} \left(u_{1i}^{(1)}, u_{12i}^{(2)} \right) \left. \right\} \\ & + \frac{1}{2}\lambda\sigma_i^{(0)} \cdot L_{2ik} \left(u_{12k}^{(2)} \right) + \mathcal{L} \int \sigma_i^{(0)} L_{11i} \left(u_{2k}^{(1)}, u_{12k}^{(2)} \right) r dr dx \end{aligned} \quad (i, j = 1, 2, \dots, 6) \quad (k, l = 1, 2, 3) \quad (20)$$

where \mathcal{L} is the unknown Lagrange multiplier, which helps to impose the orthogonality condition.

Potential Energy Function for Interactive Buckling

The potential energy under the combined action of the two modes can now be developed. The displacements are taken in the form

$$\begin{aligned} \{u\} = & \{u_1^{(1)}\}\xi_1 + \{u_2^{(1)}\}f_i(\theta)\phi_j(x)\xi_{ij} + \{u_{11}^{(2)}\}\xi_1^2 \\ & + \{u_{12}^{(2)}\}f_i(\theta)\phi_j(x)\xi_{ij}\xi_k + \{u_{22}^{(2)}\}f_i(\theta)\phi_j(x)\xi_{ij}\xi_k \end{aligned} \quad (21)$$

where $f_i(\theta)$ and $\phi_j(x)$ describe the variation of the amplitude modulating function in the circumferential and radial directions, respectively. The $\phi_j(x)$ is taken as linear over each bay and $f_i(\theta)$ is represented by a Fourier series consisting of at least three terms, viz., axisymmetric, $\cos(m\theta)$, and $\sin(m\theta)$. This results in six degrees of freedom for each element (three on the left end of the element and three on the right end of the element). Over the junction and stiffener element ϕ is taken as constant. Initial imperfections are included in the strains

$$\{\epsilon\} = L_1(u) + \frac{1}{2}L_2(u) + L_{11}(u, \tilde{u}) \quad (22)$$

where \tilde{u} represents the initial imperfections which are taken in the form of buckling modes, local and/or overall. The potential energy function is evaluated by a procedure which exploits both the orthogonality of the involved trigonometric functions and the slowly varying nature¹¹ of the overall quantities and the amplitude modulating function. The total potential energy function is obtained in the form

$$\begin{aligned} \Pi = & -\lambda b_1 \xi_1 \tilde{\xi}_1 - \lambda b_{ijkl} \xi_{ij} \tilde{\xi}_{kl} + \frac{1}{2}(a_1 - \lambda b_1)\xi_1^2 + d_1 \xi_1^4 \\ & + \frac{1}{2}(a_{ijkl} - \lambda b_{ijkl})\xi_{ij}\xi_{kl} + d_{ijklpqrs} \xi_{ij}\xi_{kl}\xi_{pq}\xi_{rs} \\ & + e_{ijkl}\xi_{ij}\xi_{kl}\xi_1 + g_{ijkl}\xi_{ij}\xi_{kl}\xi_1 \end{aligned} \quad (23)$$

The first two linear terms on right-hand side contain the contributions of initial imperfections in the overall and local modes, respectively. The quadratic terms (the third and the fifth terms, respectively) come from the buckling problem and the d' terms (the fourth and the sixth) encapsulate the postbuckling effects in individual modes. The e' and g' terms give the nonlinear coupling between the modes. Of these, the cubic terms given by e_{ijkl} arise only when the amplitude modulation is considered. These are found to be far more important than either the quartic terms or the contributions of the mixed second-order field as discussed by Sridharan and Kasagi.¹² For later discussion, the general form of Π in terms of generic degrees of freedom q_i is found to be useful,

$$\begin{aligned} \Pi = & \frac{1}{2!}(a_{ij} - \lambda b_{ij})q_i q_j + \frac{1}{3!}q_{ijkl}q_i q_j q_k q_l \\ & + \frac{1}{4!}a_{ijkl}q_i q_j q_k q_l - \lambda b_{ij}\tilde{q}_i \quad (i, j, k, l = 1, 2, \dots, N) \end{aligned} \quad (24)$$

where a_{ij} , b_{ij} , a_{ijk} , and a_{ijkl} are constants, λ is the loading parameter, and \tilde{q}_i are the imperfection parameters defined in the same sense as the degrees of freedom q_i .

Nonlinear Dynamic Analysis

General

The subject of dynamic instability encompasses many types of problems, but this study involves a structure that is suddenly loaded with a load of constant magnitude (step load) and infinite duration. The dynamic instability of shell structures which exhibit significant imperfection sensitivity due to modal interaction is considered. For loads less than the dynamic limit load, the structure will oscillate about the corresponding static equilibrium point. As the loads are increased the amplitudes of vibration become larger and, at some load (λ_D), the displacements build up without any limit.^{7,8} For imperfection-sensitive structures the dynamic buckling load λ_D is smaller than the corresponding static buckling load.

Lagrange Equations of Motion

As stated earlier, the structure is assumed to be excited in terms of its principal modes of buckling. The inertia forces associated with prebuckling displacements as well as the second-order fields are neglected.⁷

The Lagrange equations of motion for the shell can be obtained in the form

$$m_{ij}\ddot{q}_j + (a_{ij} - \lambda b_{ij})q_j + \frac{1}{2!}a_{ijk}q_jq_k + \frac{1}{3!}a_{ijkl}q_jq_kq_l - \lambda b_{ij}\ddot{q}_j = 0 \quad (25)$$

The first term in Eq. (25) is the inertial term and is related to the kinetic energy T as follows:

$$m_{ij}\ddot{q}_j = \frac{d}{dt} \left(\frac{\partial T}{\partial \dot{q}_i} \right)$$

where

$$T = \frac{1}{2} \iiint \rho(\dot{u}^2 + \dot{v}^2 + \dot{w}^2)r \, dr \, d\theta \, dx \quad (26)$$

Note that in Eqs. (25) and (26) a dot denotes differentiation with respect to time. The remaining terms in Eq. (25) are derived from the potential energy function [Eq. (24)]. The ordinary nonlinear differential equations of motion in Eq. (25) are solved by the Newmark method of time step integration¹⁶ with Newton-Raphson iterations. The initial conditions (at time = 0) are that the displacement and velocity are both equal to zero. Note that the acceleration takes a nonzero value at time = 0, because of the presence of initial imperfections and is given by

$$\ddot{q}_i = \lambda \bar{m}_{ij} b_{jk} \ddot{q}_k \quad (27)$$

where $[\bar{m}]$ matrix is the inverse of $[m]$ matrix.

Damping

The effect of damping is of interest as it can, apart from reducing the amplitudes of oscillations with time, slightly enhance the dynamic limit load. The damping is added to the structure as a

percentage of the critical damping value c_{cr} , which is defined as follows¹⁷:

$$c_{cr} = 2\sqrt{KM} \quad (28)$$

where K and M are the generalized (linear) stiffness and mass of the structure associated with a certain mode of vibration, respectively. The damping matrix is derivable from the Rayleigh dissipation function¹⁸ R

$$R = \frac{1}{2} \iiint \zeta c_{cr}(\dot{u}^2 + \dot{v}^2 + \dot{w}^2)r \, dr \, d\theta \, dx \quad (29)$$

where ζ is the damping ratio which can be given different values for the local and overall modes. Here again we neglect the contribution of the second-order terms and as a result R is a quadratic in \dot{q}_i . The dissipative forces F_i are defined as follows:

$$F_i = -\frac{\partial R}{\partial \dot{q}_i} = -c_{ij}\dot{q}_j \quad (30)$$

The Lagrange equations of motion now become

$$m_{ij}\ddot{q}_j + c_{ij}\dot{q}_j + (a_{ij} - \lambda b_{ij})q_j + \frac{1}{2!}a_{ijk}q_jq_k + \frac{1}{3!}a_{ijkl}q_jq_kq_l - \lambda b_{ij}\ddot{q}_j = 0 \quad (31)$$

Numerical Results

In this section, numerical results are presented with the following objectives in view: to demonstrate the accuracy of the finite element modeling for dynamic response and to highlight the salient features of the response of stiffened shells under the combined influence of dynamic loading and modal interaction, such as 1) the response of stiffened shells before and at the onset of instability, 2) the imperfection sensitivity of ring stiffened shells having near-coincident critical stresses, 3) the effect of damping, and 4) the buildup of

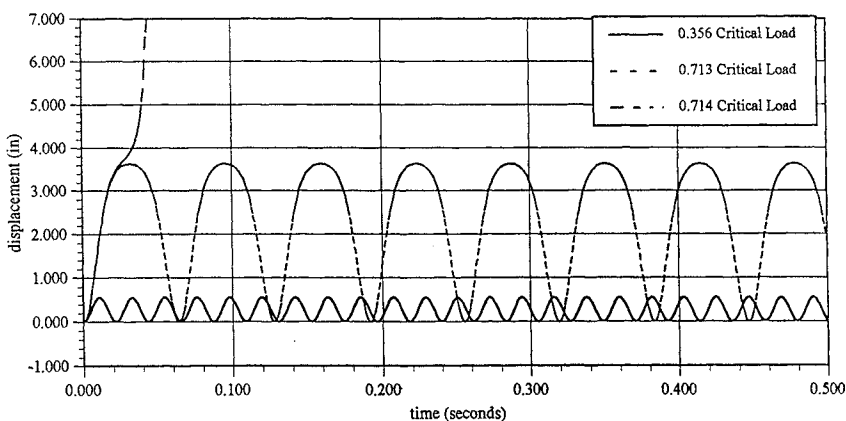


Fig. 2 Dynamic response of unstiffened composite shell, maximum displacement vs time.

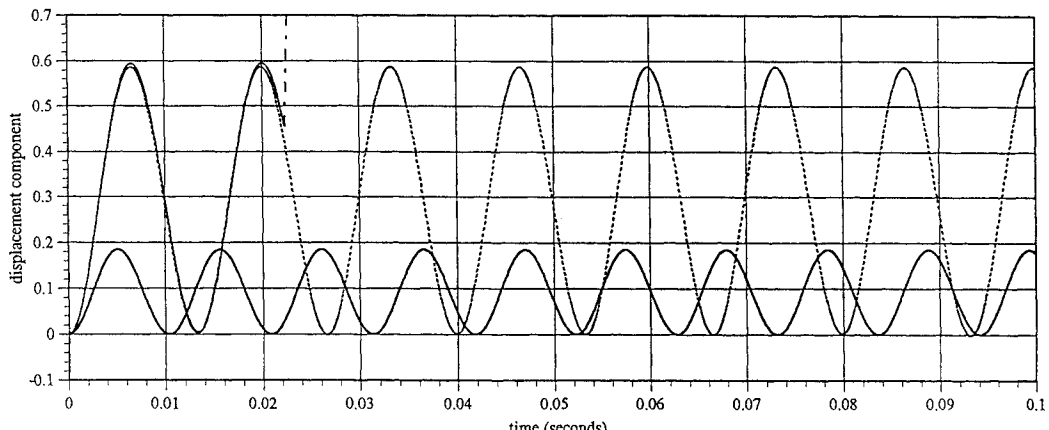


Fig. 3 Dynamic response of stiffened composite shell: amplitude of the overall buckling mode vs time: — 0.271 critical load; - - - 0.539 critical load; - - - 0.542 critical load.

Table 1 Comparison of natural frequencies ω of interior ring stiffened shell

N_s	ω , rad/s (circumferential wave number), Zhou and Yang ⁶	ω , rad/s (circumferential wave number), present study
1	0.2699 (6)	0.2672 (6)
2	0.2777 (6)	0.2749 (6)
3	0.2849 (6)	0.2820 (6)
4	0.2914 (6)	0.2886 (6)
5	0.2974 (6)	0.2945 (6)
6	0.3028 (6)	0.2999 (6)
7	0.3048 (5)	0.3038 (5)
8	0.3053 (5)	0.3045 (5)

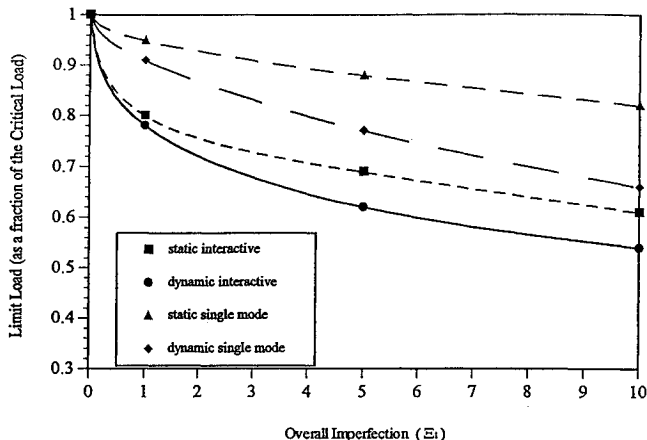


Fig. 4 Influence of modal interaction and dynamics on limit load of the composite shell carrying overall imperfection.

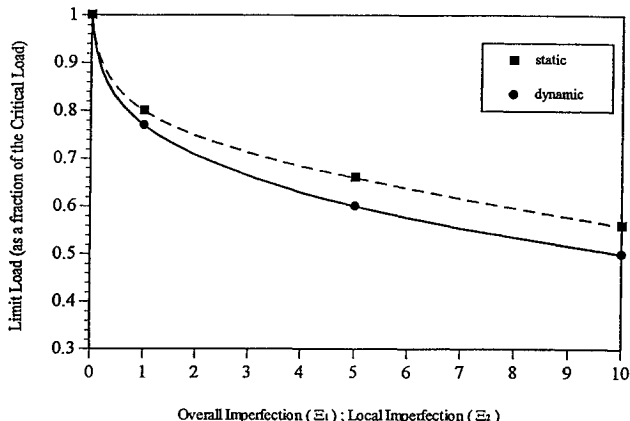


Fig. 5 Comparison of static and dynamic load carrying capacities of the isotropic shell under combined imperfections.

interlaminar stresses prior to the onset of instability. In all of the examples the shells are assumed to be simply supported at the ends, with $w = v = 0$ over the entire thickness.

Accuracy of the Finite Element Modeling

Extensive checking of the finite element modeling in the context of static buckling and postbuckling behavior has been done and reported elsewhere.^{1,2} As mentioned earlier, there is a scarcity of results for ring stiffened shells obtained from rigorous shell theories including thickness effects. Here we present a comparison of the natural frequencies of ring stiffened shells as obtained by the present model with those of Zhou and Yang⁶ who employed a discrete stiffener theory and transfer function approach for the analysis. The material of the shell is isotropic, and the number of stiffeners was varied from 1 to 8. The other parameters are as follows: $R = 100$, $L = 100$, $t = 1$, $t_s = 1$, $d = 2$, $E = 10,000$, $\nu = 0.3$, and $\rho = 10$. The results for the smallest frequencies and the corresponding wave numbers are given in Table 1. In the present model we employed fifth- and

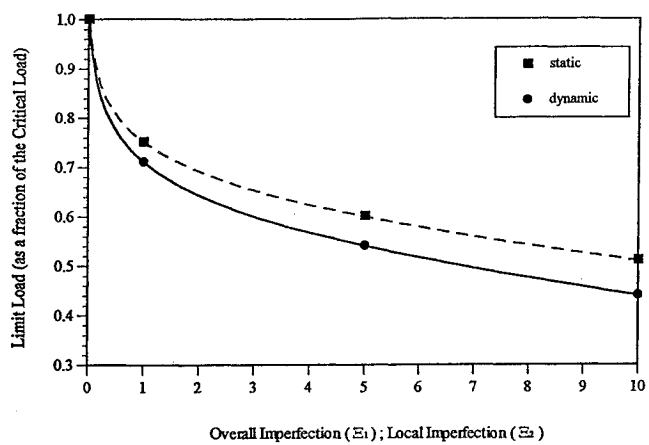


Fig. 6 Comparison of static and dynamic load carrying capacities of the composite shell under combined imperfections.

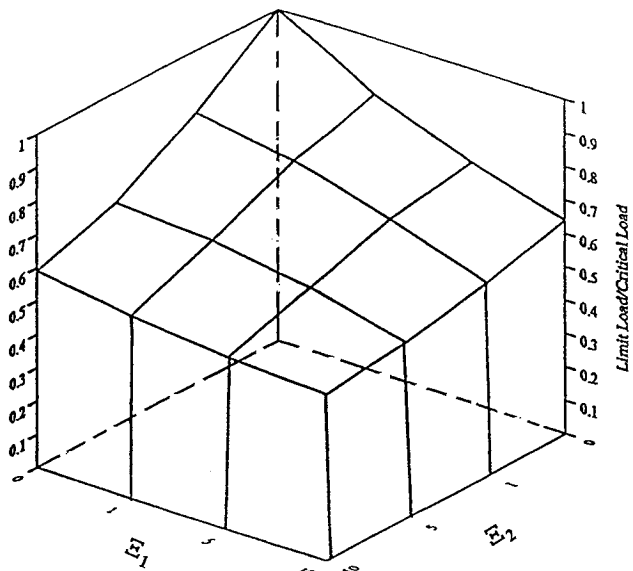


Fig. 7 Imperfection-sensitivity surface of the isotropic shell, dynamic limit load vs imperfections.

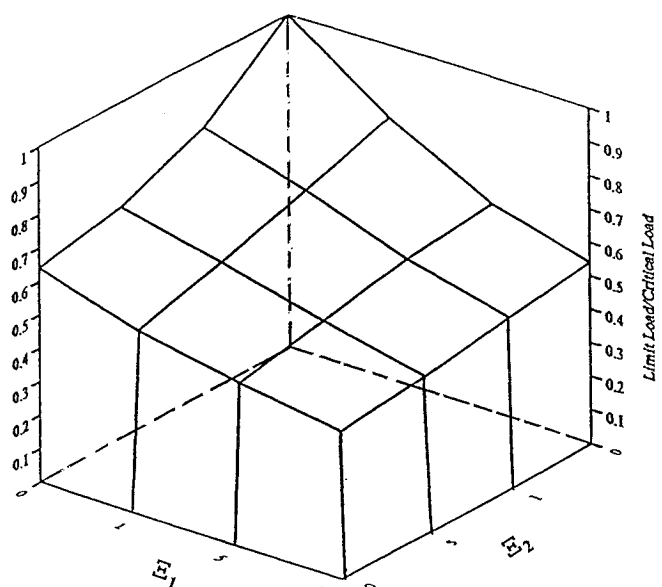


Fig. 8 Imperfection-sensitivity surface of the composite shell, dynamic limit load vs imperfections.

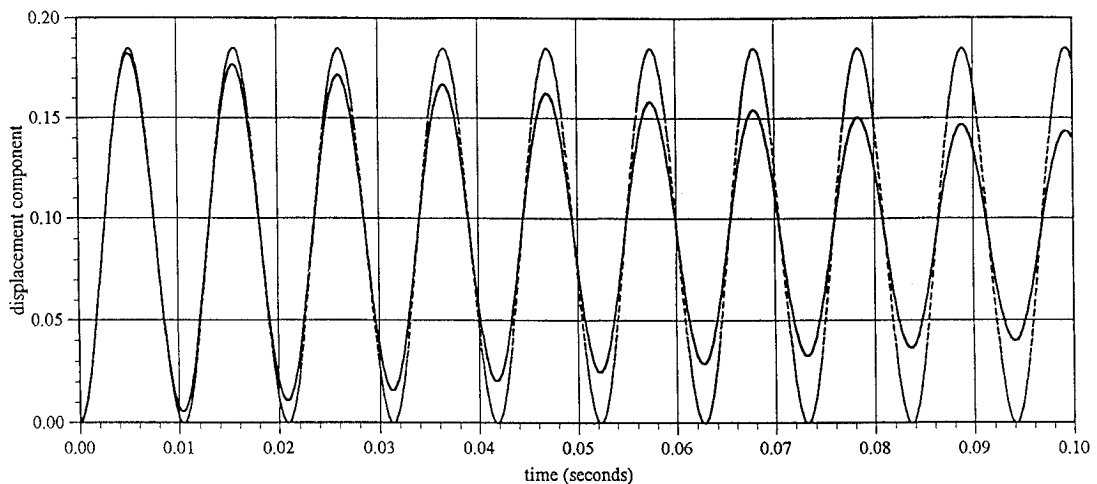


Fig. 9 Influence of 1% damping on the dynamic response of the composite shell at $\lambda = 0.271\lambda_{cr}$ with $\Xi_1 = \Xi_2 = 5$: - - - 0% damping; — 1% damping.

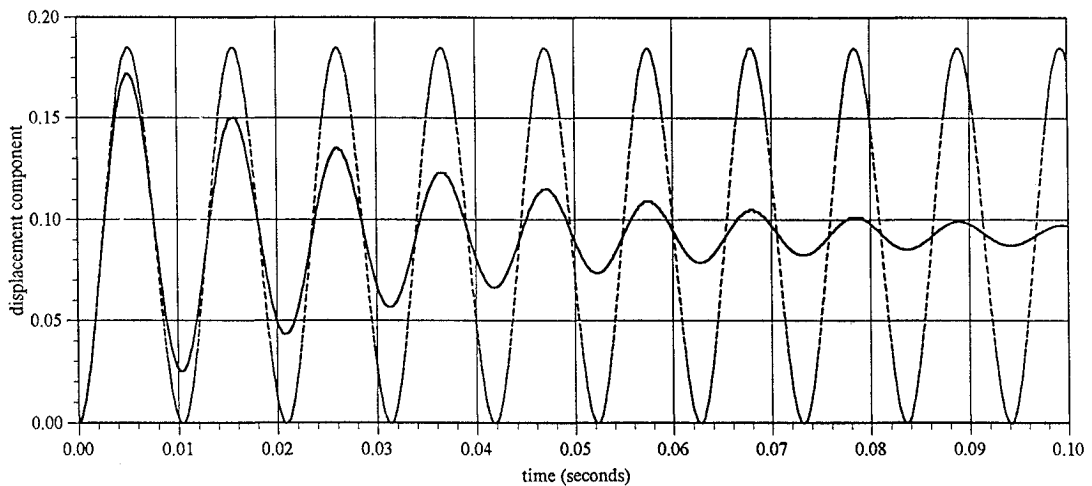


Fig. 10 Influence of 5% damping on the dynamic response of the composite shell at $\lambda = 0.271\lambda_{cr}$ with $\Xi_1 = \Xi_2 = 5$: - - - 0% damping; — 5% damping.

third-degree polynomials in the longitudinal and thickness direction, respectively, in each of the elements, and this produced a converged result to the fourth digit. Despite a number of differences between the two approaches, it is seen that the results are very close indeed.

Nonlinear Dynamic Response

Geometry and Material Properties

Interactive buckling is considered for shells having nearly co-incident local and overall critical loads. Isotropic and orthotropic interior ring stiffened shells are considered with the following geometric and material properties (all material constants are given in pounds per square inch).

For Shell 1 the material is isotropic with $E = 10 \times 10^6$, $G = 3.85 \times 10^6$, $\nu = 0.3$, and $\rho = 0.147 \times 10^{-3}$. The geometry is defined as $R = 50$ in., $L/R = 4.64$, $R/t = 62.5$, $t_s/t = 1.5$, $d/t_s = 4.792$, $S_p/R = 0.400$, and $N_s = 10$. The critical stresses are $\lambda_{cr}^{(1)}/E = 1.17 \times 10^{-4}$ and $\lambda_{cr}^{(2)}/E = 1.17 \times 10^{-4}$.

For shell 2 the material is specially orthotropic¹⁹ with $E_{11} = 16.0 \times 10^6$, $E_{22} = 1.48 \times 10^6$, $E_{33} = 1.48 \times 10^6$, $\nu_{12} = 0.33$, $\nu_{13} = 0.33$, $\nu_{23} = 0.33$, and $\rho = 0.147 \times 10^{-3}$. The geometry is defined as a [90/0], laminate with $R = 50$ in., $L/R = 2.62$, $R/t = 100$, $t_s/t = 2.0$, $d/t_s = 2.711$, $S_p/R = 0.220$, and $N_s = 10$. The critical stresses are $\lambda_{cr}^{(1)}/E_{11} = 1.90 \times 10^{-5}$ and $\lambda_{cr}^{(2)}/E_{11} = 1.89 \times 10^{-5}$.

Imperfection Parameters

Two imperfection parameters, viz., Ξ_1 and Ξ_2 are introduced to give the magnitude of imperfections in the sense of overall and local modes, respectively. The maximum overall and local imperfections

considered in the present work are $t/10$ and $R/100$, respectively, and these correspond to values of 10 and 10 for Ξ_1 and Ξ_2 , respectively.

Description of the Response

For loads below the dynamic limit load the displacements remain bounded and oscillate around a certain value. As the load is increased, the amplitude of vibration increases while the frequency decreases significantly. Figure 2 illustrates this behavior for an unstiffened orthotropic shell ($R = 50$ in., $L/R = 4$, $t = 1$ in., $\Xi_1 = 10$, otherwise having the same data as shell 2) which is governed by a single mode. The response curve with the smallest amplitude is drawn for a load of one-half of the dynamic limit load, and the response curve with the larger amplitude is for a load just under the dynamic limit load. When the dynamic limit load is reached, the displacements immediately become unbounded before any oscillations occur. A different behavior, however, is observed for the stiffened orthotropic shell (shell 2) under interactive buckling. When the limit load is reached, the displacement amplitudes of the overall mode complete a few oscillations before heading toward infinity as shown in Fig. 3.

Reduction of Buckling Pressure Under Modal Interaction

The stiffened shell (shell 2) is further investigated to study the effects of dynamic loading and mode interaction on the buckling pressure of the shell. Figure 4 illustrates these reductions when considering only overall imperfections in the interactive analysis with minute local imperfections to circumvent a dynamic bifurcation. The top two curves show the reductions as found from a single mode analysis whereas the bottom two curves show the reduction due to

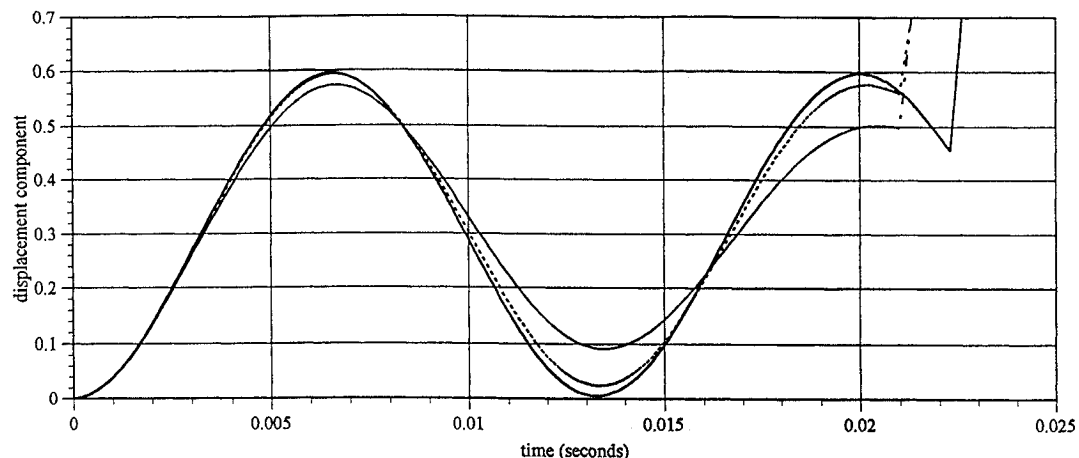


Fig. 11 Influence of damping on the dynamic response and limit load of the composite shell with $\Xi_1 = \Xi_2 = 5$: — 0% damping (0.542 critical load); - - - 1% damping (0.546 critical load); - - - 5% damping (0.552 critical load).

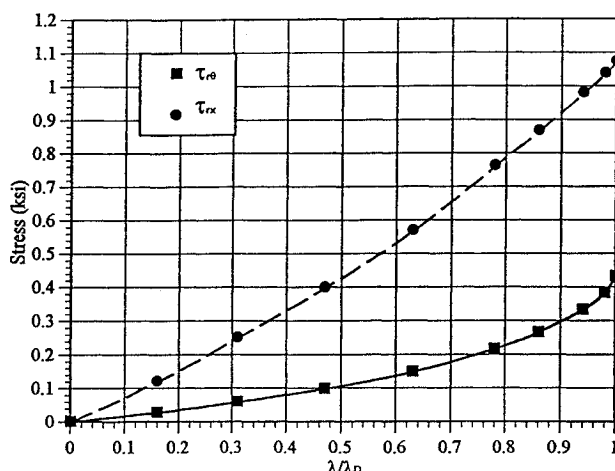


Fig. 12 Variation of interlaminar stresses at selected locations of the composite shell ($\Xi_1 = \Xi_2 = 5$) with load.

the interactive analysis. In the range of imperfections investigated, the curves show that the load reduction increases monotonically with imperfection magnitudes. Figures 5 and 6 show the reduction due to dynamic loading for the two shells (1 and 2) carrying imperfections in both the local and overall modes, such that $\Xi_1 = \Xi_2$. The reduction is significant in each case, the maximum load reducing to just 44% of the critical load for the orthotropic case.

Figures 7 and 8 show the variation of dynamic limit load with imperfection magnitudes as given by Ξ_1 and Ξ_2 , respectively, for the two stiffened shells under study. Unlike in Figs. 5 and 6, Ξ_1 and Ξ_2 are freely varied. These figures—often called imperfection-sensitivity surfaces—tend to be rather steep for small imperfections and flatten out as imperfections increase.

Influence of Damping

In practice, some damping is inherent in a shell. Damping percentages of 1–2% are likely. In this study, damping percentages of 1% and 5% are used for illustration, and damping is only added in the overall mode. Considering shell 2 under combined imperfection ($\Xi_1 = \Xi_2 = 5$) the reduction in the overall displacement amplitude is shown in Figs. 9 and 10 for 1% and 5% damping, respectively. The oscillations get damped out rather quickly in the latter case. The effect of damping on the dynamic limit load is shown in Fig. 11. For each case, the shell undergoes several oscillations before the displacements become unbounded. For both 1% and 5% damping, the dynamic limit load is only slightly increased and, thus, the damping has little effect on the dynamic limit load.

Interlaminar Stresses

It is possible that the large-amplitude vibrations that precede the onset of dynamic instability will cause some form of material failure

cutting short the maximum load carrying capacity of the structure. Since delamination is a common type of failure of laminated shells we pay special attention to interlaminar stresses. Figure 12 shows the interlaminar shear stresses for the composite shell 2 with imperfections in both the local and overall modes ($\Xi_1 = \Xi_2 = 10$). The $\tau_{r\theta}$ stresses are considered at the center of the shell between the outermost 0 and 90-deg layers at $\theta = 45$ deg. The τ_{rx} stresses are considered at the junction nearest the center between the two 0-deg layers at $\theta = 0$ deg. The interlaminar stresses reach values above 1 ksi prior to attaining the dynamic limit load, values which may be considered high for many composite materials. To predict delamination in a practical context, however, these values must be used in conjunction with an appropriate failure criterion and the presence of pre-existing delaminations and voids.

Conclusions

The dynamic limit load of an imperfect composite cylindrical shell can be significantly lower than the static limit load under modal interaction. The dynamic limit load is reduced to as low as 44% of the critical load of the perfect shell for the coincident buckling case. For loads below the dynamic limit load, the shell oscillates with amplitudes which rapidly increase with the applied pressure. When the dynamic limit load is reached, the displacements immediately become unbounded for single-mode analysis. However, for interactive analysis of a stiffened shell, the displacements undergo several oscillations before becoming unbounded. The effects of damping on the dynamic limit load of the shell are minimal for the percentages of damping found in practice. The interlaminar stresses reach substantial values before the dynamic limit load is reached, something which can be a cause for concern in practical design.

Acknowledgments

The research contained in this paper was supported by the Office of Naval Research under Grant N00014-91-J1637 of the Ship Structures and Systems Science and Technology Division of the Solid Mechanics Program. The constant interest and encouragement of Yapa D.S. Rajapakse, the program director, is greatly appreciated.

References

- Kasagi, A., and Sridharan, S., "Buckling and Postbuckling Analysis of Thick Composite Cylindrical Shells Under Hydrostatic Pressure," *Composites Engineering*, Vol. 3, No. 5, 1993, pp. 467–487.
- Kasagi, A., "Interactive Buckling of Ring Stiffened Composite Cylindrical Shells," D.Sc. Thesis, Dept. of Civil Engineering, Washington Univ., St. Louis, MO, May 1994.
- Jones, R. M., and Morgan, H. S., "Buckling and Vibration of Cross-Ply Laminated Circular Cylindrical Shells," *AIAA Journal*, Vol. 13, No. 5, 1975, pp. 664–671.
- Simitses, G. J., Tabiei, A., and Anastasiadis, J. S., "Buckling of Moderately Thick, Laminated Cylindrical Shells Under Lateral Pressure," *Composites Engineering*, Vol. 3, No. 5, 1993, pp. 409–417.

⁵Langley, R. S., "A Dynamic Stiffness Technique for the Vibration Analysis of Stiffened Shell Structures," *Journal of Sound and Vibration*, Vol. 156, No. 3, 1992, pp. 521-540.

⁶Zhou, J., and Yang, B., "Analysis of Ring-Stiffened Shells," *Journal of Applied Mechanics* (to be published).

⁷Budiansky, B., "Dynamic Buckling of Elastic Structures: Criteria and Estimates," *Dynamic Stability of Structures*, edited by G. Herrman, Pergamon Press, Oxford, England, UK, 1966, pp. 83-106.

⁸Simitses, G. J., *Dynamic Stability of Suddenly Loaded Structures*, Springer-Verlag, New York, 1989, pp. 24-53.

⁹Palazotto, A. N., Chien, L. S., and Taylor, W. W., "Stability Characteristics of Laminated Cylindrical Panels Under Transverse Loading," *Proceedings of the AIAA/ASME/ASCE/AHS/ASC 32nd Structures, Structural Dynamics, and Materials Conference* (Baltimore, MD), Pt. 2, AIAA, Washington, DC, 1991, pp. 926-937.

¹⁰Koiter, W. T., "General Theory of Mode Interaction in Stiffened Plate and Shell Structures," Delft Univ. of Technology, Rept. WTHD-91, Delft, The Netherlands, 1976.

¹¹Sridharan, S., Madjid, Z., and Starnes, J. H., Jr., "Mode Interaction Analysis of Stiffened Shells Using Locally Buckled Elements," *International Journal of Solids and Structures*, Vol. 31, No. 17, 1994, pp. 2347-2366.

¹²Sridharan, S., and Kasagi, A., "Interactive Buckling in Composite Cylinders," *Proceedings of the AIAA/ASME/ASCE/AHS/ASC 35th Structures, Structural Dynamics, and Materials Conference* (Hilton Head, SC), Pt. 1, AIAA, Washington, DC, 1994, pp. 299-308.

¹³Szabó, B. A., and Babuška, I., *Finite Element Analysis*, Wiley, New York, 1991, pp. 98, 99.

¹⁴Dyau, J. Y., and Kyriakides, S., "On the Propagation Pressure of Long Cylindrical Shells Under External Pressure," *International Journal of Mechanical Science*, Vol. 35, No. 8, 1993, pp. 675-713.

¹⁵Koiter, W. T., "On the Stability of Equilibrium," (in Dutch), Thesis, Delft Inst. of Technology, 1945; English Translation, NASA, Tech. Trans., F-10,833, 1967, pp. 1-100.

¹⁶Bathe, K. J., *Finite Element Procedures in Engineering Analysis*, Prentice-Hall, Englewood Cliffs, NJ, 1982, pp. 499-556.

¹⁷Paz, M., *Structural Dynamics, Theory and Computation*, Van Nostrand Reinhold, New York, 1985, pp. 24, 25.

¹⁸Huseyin, K., *Vibrations and Stability of Multiple Parameter Systems*, Sijthoff and Noordhoff International, Publishers, Alphen aan den Rijn, The Netherlands, 1978, pp. 58, 59.

¹⁹Sun, C. T., and Sijian, L., "Three-Dimensional Effective Elastic Constants for Thick Laminates," *Journal of Composite Materials*, Vol. 22, No. 7, 1988, pp. 629-639.